Supporting Information

Screen-Printing Fabrication of High Volumetric Energy Density Micro-Supercapacitors based on High-Resolution Thixotropic-Ternary Hybrid Interdigital Micro-Electrodes

Hongpeng Li[a], Shuiren Liu[a], Xiran Li[a], Zhong-Shuai Wu*[d], and Jiajie Liang *[abc]

[a] School of Materials Science and Engineering, National Institute for Advanced Materials Nankai University, Tianjin 300350, PR China.

[b] Key Laboratory of Functional Polymer Materials of Ministry of Education, College of Chemistry, Nankai University, Tianjin 300350, PR China.

[c] Tianjin Key Laboratory of Metal and Molecule-Based Material Chemistry and Collaborative Innovation Center of Chemical Science and Engineering (Tianjin), Nankai University, Tianjin 300350, PR China.

[d] Dalian National Laboratory for Clean Energy, Dalian Institute of Chemical Physics, Chinese Academy of Sciences, 457 Zhongshan Road, Dalian 116023, China

Email: liang0909@nankai.edu.cn (J. Liang); wuzs@dicp.ac.cn (Z.-S. Wu).

Calculations: The capacitance values were calculated from the CV curves by integrating the discharge portion using the following equation:[1,2]

$$C = \frac{1}{\nu(V_f - V_i)} \int_{V_i}^{V_f} I(V)dV \tag{1}$$

where V_f and V_i are the integration potential limits of the voltammetric curve, ν is the scan rate (V s^{-1}), and I(V) is the voltammetric discharge current (A).

The capacitance values was calculated from the galvanostatic charge/discharge curves using the following equation:

$$C = \frac{I \times \Delta t}{\Delta V} \tag{2}$$

where I is the discharge current (A), Δt is the time in seconds of the discharge (s), and ΔV is the discharge potential range (V).

Areal and volumetric specific capacitance of the MSC device was calculated based on the area and volume of the device according to the following formulas (3) and (4):

$$C_{areal} = C / A_{device} \tag{3}$$

$$C_{vol} = C / V_{device} \tag{4}$$

where C_{areal} (F cm^{-2}) and C_{vol} (F cm^{-3}) refer to the areal specific capacitance and volumetric specific capacitance of the MSC device, respectively. A_{device} and V_{device} are the total area and volume of the device (including the interdigitated electrodes and the interspace between them), respectively.

Additionally, the volumetric energy density (E) and power density (P) of the MSC device are calculated by the following equations, respectively:

$$E = \frac{1}{2} \times C_{vol} \times \frac{(\Delta V)^2}{3600} \tag{5}$$

$$P = \frac{E}{\Delta t} \times 3600 \tag{6}$$

where E is the volumetric energy density (Wh cm^{-3}), where P is the volumetric power density (W cm^{-3}), C_{vol} is the volumetric specific capacitance obtained from formula (3), ΔV is the discharge potential range (V), and Δt is the discharge time (s).

	MSC-4-200	MSC-4-150	MSC4-100	MSC-4-50
Width (μm)	200	150	100	50
Interspace (μm)	100	100	100	100
Length (mm)	5	5	5	5
Edge (μm)	150	150	150	150
Device area (cm^3)	0.47615	0.3959	0.31565	0.2354

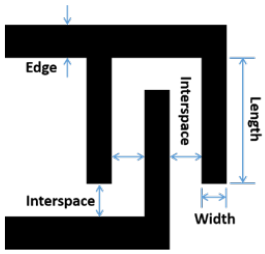

Figure S1. Dimensions and schematic diagram of the interdigitated electrodes of the fabricated micro-supercapacitor (MSC).

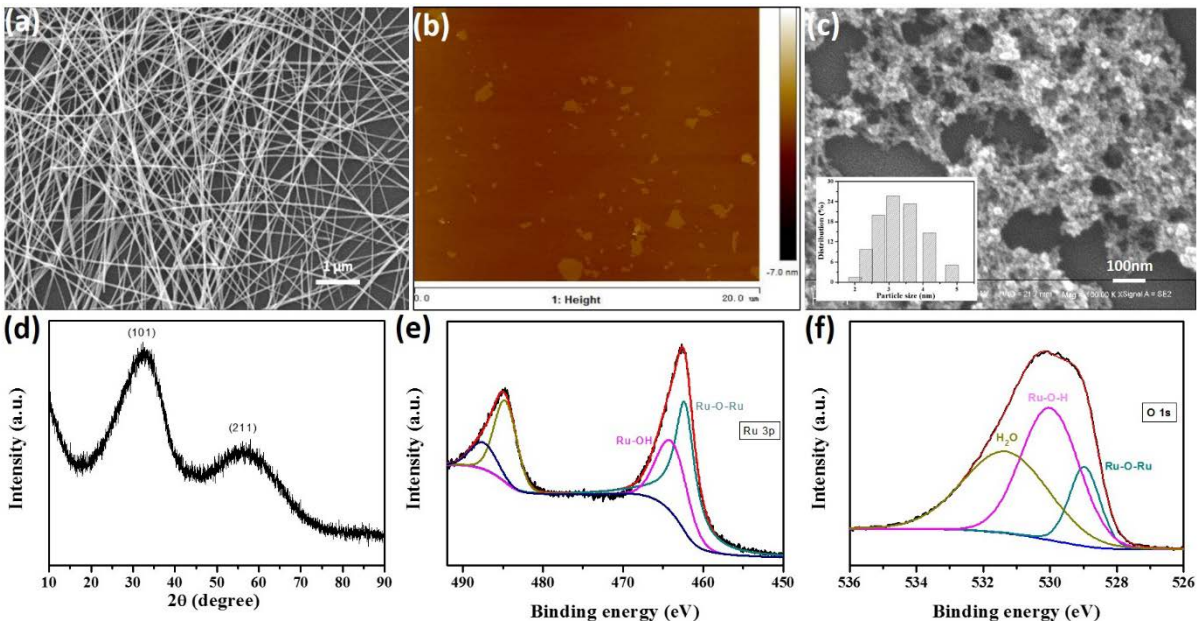

Figure S2. Structural and chemical characterization of the raw materials for screen printing ink: (a) SEM image of AgNW, (b) AFM image of GO nanosheet, (c) SEM image of hydrous RuO_2 nanoparticles. XRD pattern (d), high-resolution XPS spectra of Ru 3p (e) and O 1s (f) originating from hydrous RuO_2. The inset of (c) is the histogram of the hydrous RuO_2 particle size distribution.

Structural and chemical characterization of raw materials for the screen printing ink are presented in Figure S2. The top-view SEM image of AgNWs in Figure S2a shows the average diameter of AgNWs is ~30 nm (diameters range from 25 to 35 nm), and the average length is ~20 μm (lengths range from 15 to 25 μm). The morphology of the GO nanosheets was investigated by AFM as shown in Figure S2b. Note that the average lateral size of the GO nanosheets was about 1 μm, which is ideal for the screen printing techniques, as larger graphene sheets may block the screen mesh. Hydrous RuO_2 nanoparticles were synthesized with the sol-gel method and subsequently heat-treated at 150 °C for 1 h. The average size of as-prepared hydrous RuO_2 nanoparticles is ~3.2 nm, which is confirmed by the SEM image and the

histogram (Figure S2c). The broad XRD diffuse pattern in Figure S2d confirms the amorphous nature of hydrous RuO_2 obtained by annealing at a low temperature of 150 °C.[3,4]

X-ray photoelectron spectroscopy (XPS) is always used to identify oxidation states and hydrous nature of the obtained RuO_2 nanoparticles. Typical XPS spectrums of Ru 3p and O 1s core-level electrons for hydrous RuO_2 prepared by sol-gel method are shown in Figure S2e and S2f. As shown in Figure S2e, the Ru 3p spectrum consists of two core level spectrum peaks at 484.8 eV and 462.7 eV, corresponding to the Ru $3p_{1/2}$ and Ru $3p_{3/2}$ spin orbit lines respectively, which are assigned to ruthenium (IV) oxide.[5] Furthermore, the Ru $3p_{3/2}$ peak can be deconvoluted into two components, which are identified as Ru-OH (463.8 eV) and RuO_2 (462.3 eV).[6] In the O 1s core level spectrum (Figure S2f), three sections can be fitted: the peak at 530.0 eV is attributed to Ru-O-Ru bond, the major peak centered at 529.0 eV is associated with functional group of Ru-O-H and the peak observed at 531.4 eV is the contribution of water.[7] According to a previous report,[8,9] the low crystallinity hydrous RuO_2 with high density of surface hydroxyl groups not only provides very facile pathways for electron and proton transports, but also enhances the electronic conductivity for the redox transitions of electrochemical activity species.

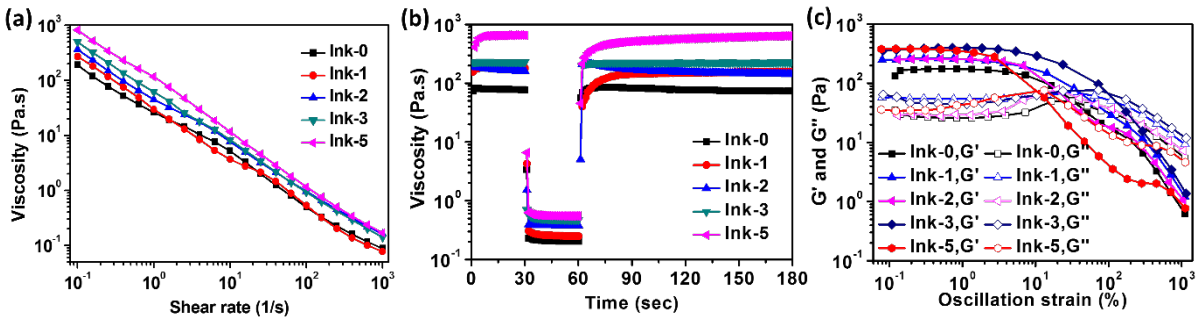

Figure S3. Rheological behaviors of Ink-0, Ink-1, Ink-2, Ink-3 and Ink-5. (a) Viscosity as a function of shear rate. (b) Rheological behavior of the ink during the screen printing process. (c) Variation of storage modulus (G′) and loss modulus (G″) as a function of oscillation strain.

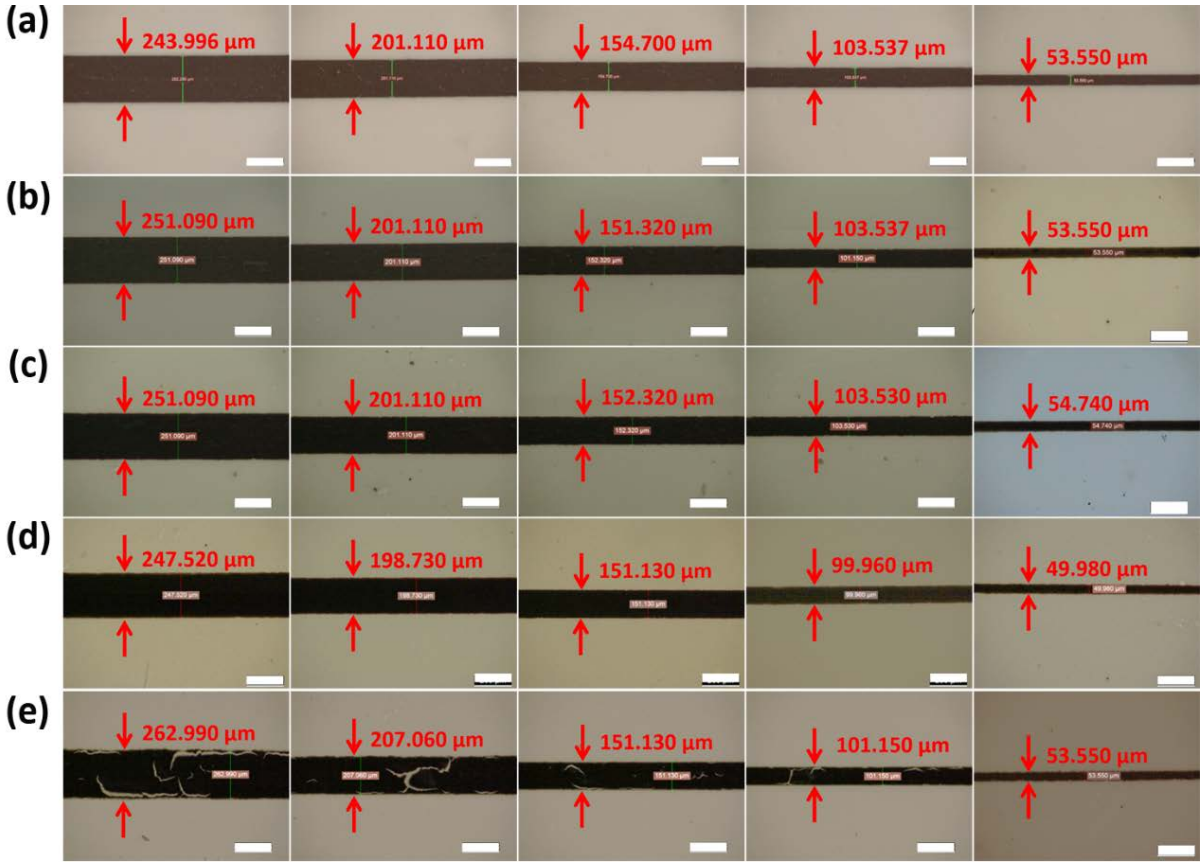

Figure S4. Optical microscopy images of screen-printed electrodes lines with various line widths based on (a) Ink-0 ink, (b) Ink-1 ink, (c) Ink-2 ink, (d) Ink-3, and (e) Ink-5. 250 µm, 200 µm, 150 µm, 100 µm, and 50 µm wide stencil openings (from left to right) were used in (a)-(e). The scale bar in each image is 200 µm.

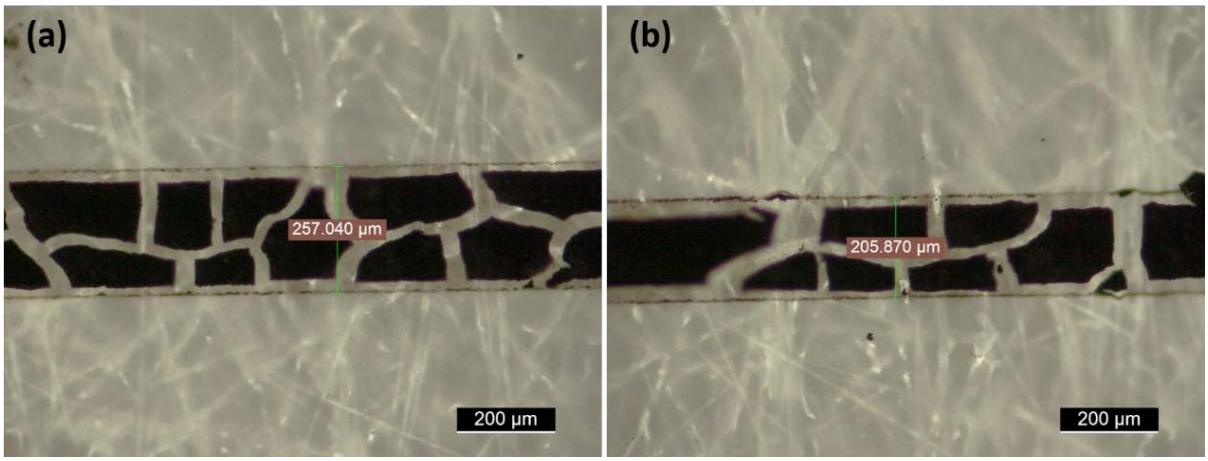

Figure S5. Optical microscopy images of screen-printed lines printed on filter paper substrates based on Ink-6 ink with line widths of (a) 250 and (b) 200 µm.

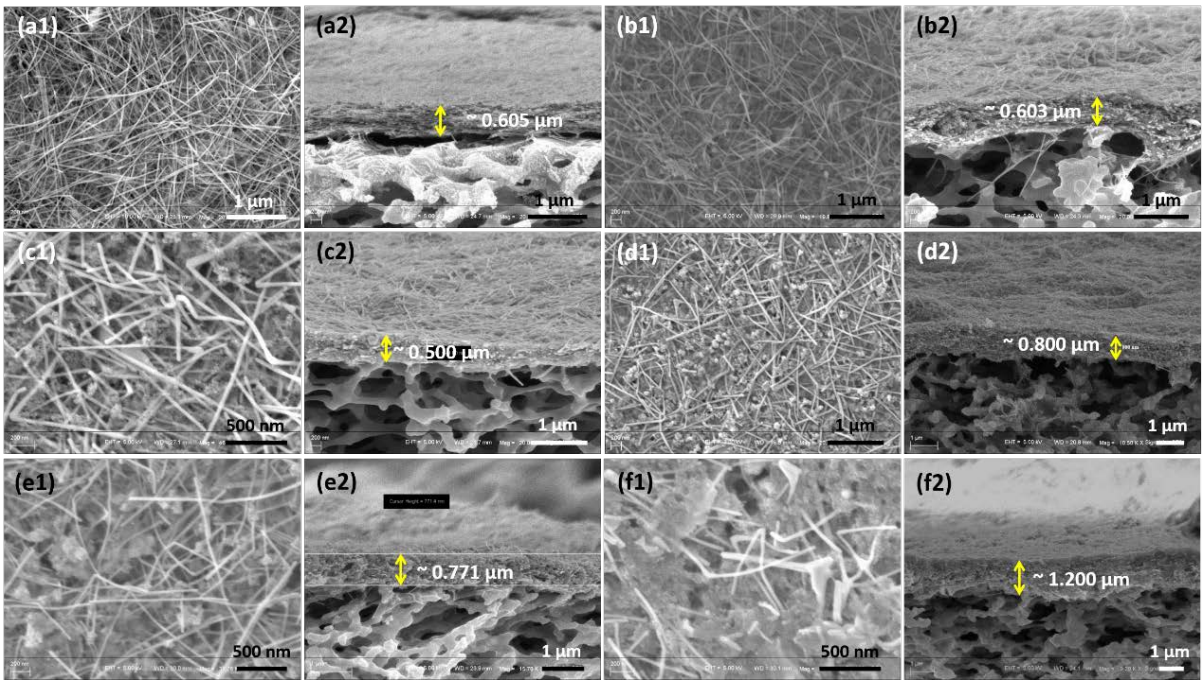

Figure S6. Top-view and cross-sectional SEM images of screen-printed interdigital type electrodes (width: 200 µm) of obtained by (a1, a2) RArG-0 MSC, (b1, b2) RArG-1 MSC, (c1, c2) RArG-2 MSC, (d1, d2) RArG-3 MSC, (e1, e2) RArG-4 MSC, and (f1, f2) RArG-5 MSC.

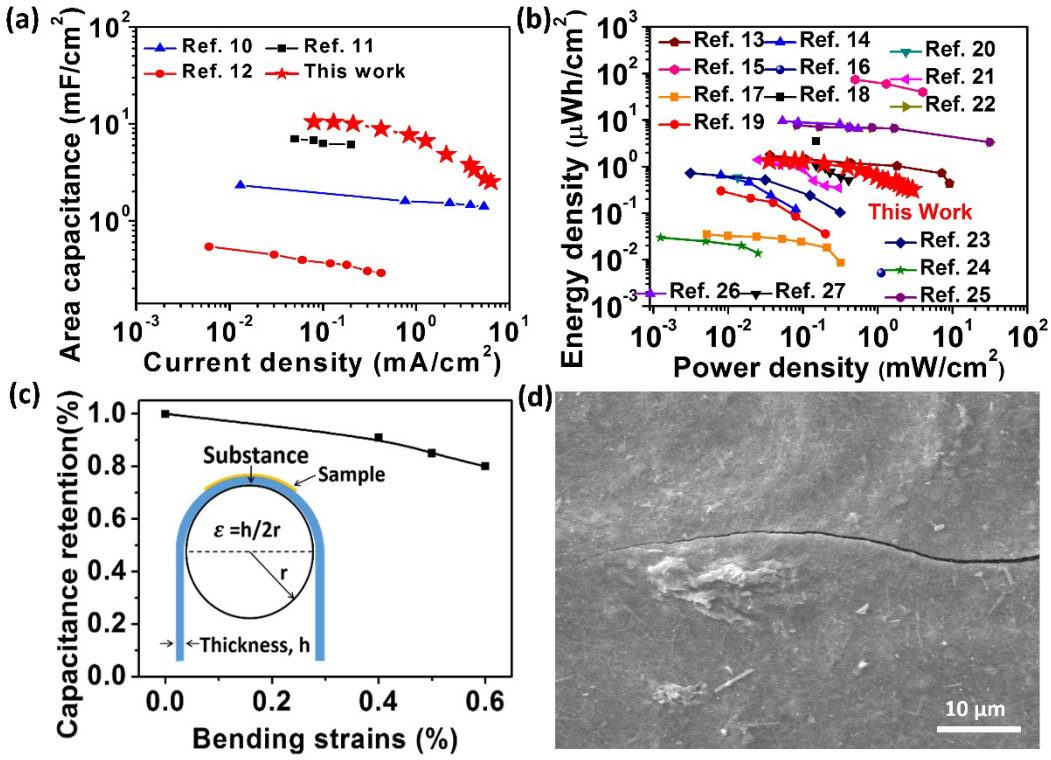

Figure S7. (a) Areal specific capacitance calculated from different current densities of RArG-4-200 MSC device in comparison to other state-of-the-art microsupercapacitors fabricated by conventional microfabrication methods. (b) Areal Ragone plot of RArG-4-200 MSC device in comparison to other state-of-the-art microsupercapacitors fabricated by printing methods. (c) Capacitance retention of RArG-4-200 MSC under different bending strains at a scan rate of 100 mV s^{-1}. (d) Top-view SEM image of RArG-4-200 micro-electrode after 2,000 bending. The inset of (c) is schematic illustration of the bending test method.

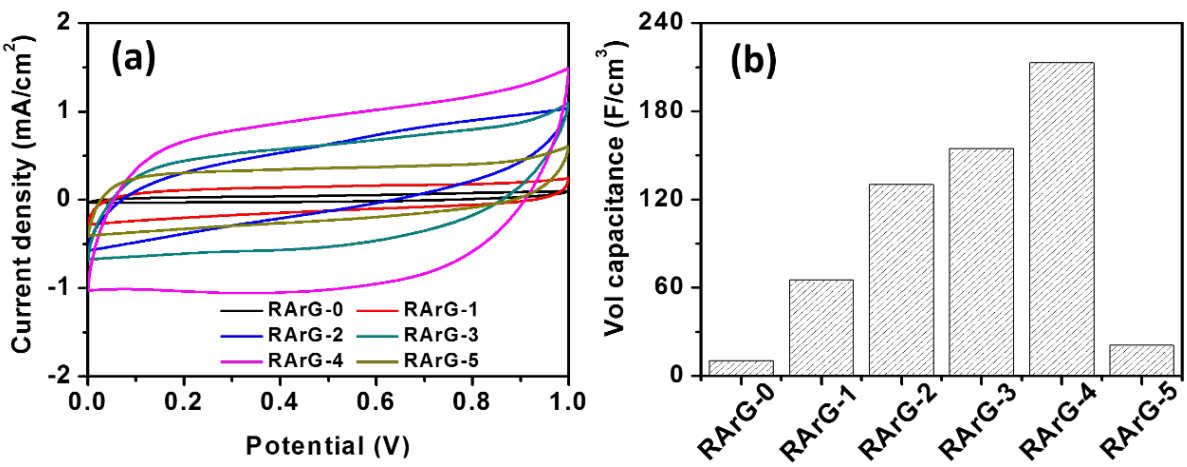

Figure S8. (a) CV curves and (b) corresponding volumetric specific capacitance histogram obtained at a scan rate of 100 mV s^{-1} for RArG MSCs (interdigital electrodes width: 200 μm) with different contents of hydrous RuO_2.

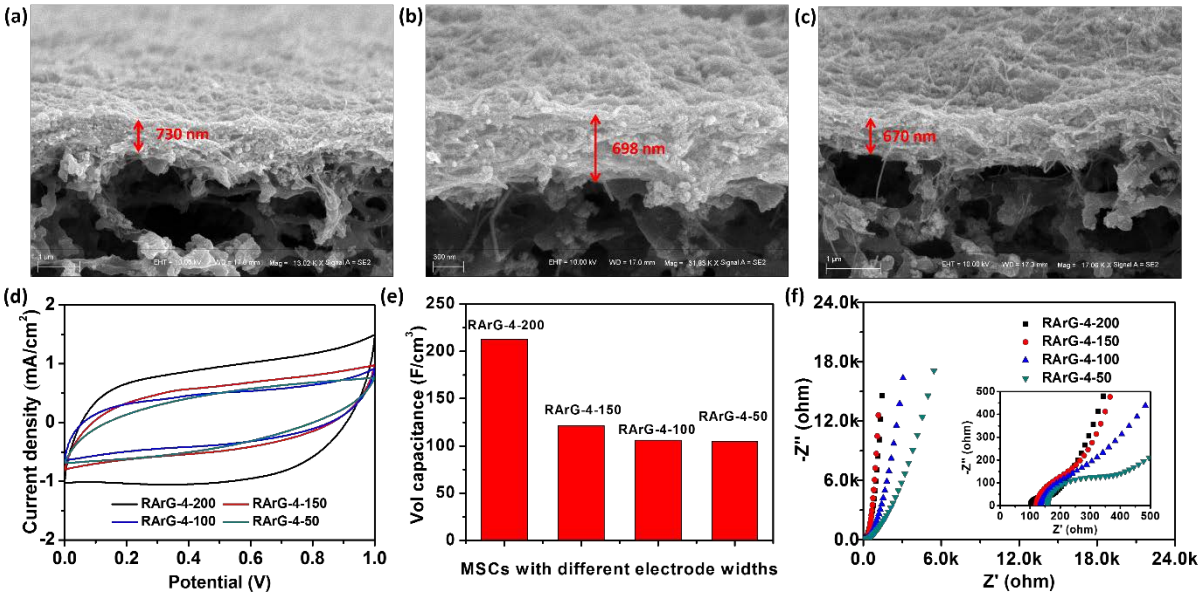

Figure S9. Cross-sectional SEM images of screen-printed interdigital type electrodes of (a) RArG-4-150 MSC, (b) RArG-4-100 MSC, (c) RArG-4-50 MSC. Electrochemical performances of RArG-4 MSCs with different widths of the figure electrodes: (d) CV curves and (e) corresponding volumetric specific capacitance obtained at a scan rate of 100 mV s^{-1}; (f) Nyquist plots.

According to a guidelines paper published by Gao's group,[1] the electrochemical performances of the microsupercapacitors with in-plane interdigital electrode architecture are depended on the the ratio of W_e/W_i, where W_e is the with width and W_i is the width of interspace between adjacent electrodes. When the ionic conductivity of electrolyte and the width of interspace are fixed, increasing the ratio of W_e/W_i can efficiently decrease the equivalent series resistance (ESR) and enhance electrochemical performances. As seen in Figure S9f, the RArG-4-200 has smaller ESR than others. In addition, compared with other MSCs, RArG-4-200 has more electrochemical active materials because of the wider electrode. As a result, the RArG-4-200 higher specific volume capacitance then narrower.

Table S1. Comparison of the electrochemical performances normalized based on geometric area and volume of MSCs fabricated employing various printing techniques.

References	Preparation Method	System	Thickness (μm)	Areal Capacitance (mF cm^{-2})	Volumetric Capacitance (F cm^{-3})	Areal Power Density (mW cm^{-2})	Areal Energy Density (μWh cm^{-2})	Volumetric Power Density (W cm^{-3})	Volumetric Energy Density (mWh cm^{-3})
13	3D printing	GO/PA-PE	4.5	15.5 (5 mV s^{-1})	34.5 (5 mV s^{-1})	-	1.42	-	3.16
		GO/PAPE	80	153.6 (5 mV s^{-1})	19.2 (5 mV s^{-1})	-	15.4	-	1.92
		GO/PANi-PEDOT:PSS	3.6	9 (5 mV s^{-1})	25 (5 mV s^{-1})	9.1	1.74	25.3	4.83
14	Screen printing	MnO_2/onion like carbon	10	7.04 (20 uA cm^{-2})	7.04 (20 uA cm^{-2})	0.08	0.65	0.08	0.65
15	3D printing	VOx/rGO and G-VNQDs/rGO	415.8	207.9 (0.63 mA cm^{-2})	5.0 (0.63 mA cm^{-2})	~4	73.9	~0.098	1.802
16	Inkjet printing	graphene/ethyl cellulose	0.04	0.0372 (0.25 A cm^{-3})	9.3 (0.25 A cm^{-3})	1.12	0.00516	278	1.29
17	Inkjet printing	Graphene	0.35	0.268 (10 mV s^{-1})	7.66 (10 mV s^{-1})	0.32	0.035	9.1	1
18	Screen printing	CoO/CNT nanocomposite	~10	-	17.4 (0.25 A cm^{-3})	-	3.48	-	3.48
19	Screen printing	N-doped rGO	10	3.4 at (20 μA cm^{-2})	3.4 (20 μA cm^{-2})	0.2	0.3	0.2	0.3
20	Gravure printing	MoS_2@S-rGO	10	6.56 (75 uA cm^{-2})	6.56 (75 uA cm^{-2})	0.0134	0.583	0.0134	0.583

21	Gravure printing	$Mg(OH)_2$/GO	10	6.65 (0.1 mA cm^{-2})	6.65 (0.1 mA cm^{-2})	0.3	1.41	0.3	1.41
22	3D printing	Graphene	~560 (4 layers)	56.7 (5 mV s^{-1})	1 (5 mV s^{-1})	31.7	7.8	0.566	0.14
			~1330 (8 layers)	74.31 (5 mV s^{-1})	0.56 (5 mV s^{-1})				
23	3D printing	rGO	~1.04 (1 layer)	~3.3 (0.6 A cm^{-3})	~32 (0.6 A cm^{-3})	0.312	0.728	~3	7
			~2.08 (2 layers)	11.752 (0.06 A cm^{-3})	56.5 (0.06 A cm^{-3})	-	-	-	-
24	Inkjet printing	Exfoliated graphene	0.25	~0.23 (0.06 A cm^{-3})	~3.1 (0.06 A cm^{-3})	0.025	0.03	~1	~1.2
			0.75	0.7 (10 mV s^{-1})	9.3 (10 mV s^{-1})	-	-	-	-
25	Inkjet printing	PEDOT:PSS-CNT	0.051	0.12 (10 mV s^{-1})	23.6 (10 mV s^{-1})	1.07	0.0153	~210	~3
			0.628	0.44 (10 mV s^{-1})	7 (10 mV s^{-1})	3.14	0.0504	~50	~0.8
26	Inkjet printing	$K_2Co_3(P_2O_7)_2 \cdot 2H_2O$ and graphene	1.2	0.74 (10 mA cm^{-3})	6.0 (10 mA cm^{-3})	0.00654	0.115	0.0545	0.96
27	Inkjet printing	rGO	10	0.63 (2 μA)	0.63 (2 μA)	0.408	1.06	0.408	1.06
This work	**Screen printing**	**RuO_2/AgNW/rGO**	**0.71**	**26 (1 mV s^{-1})**	**338 (1 mV s^{-1})**	**2.9**	**1.33**	**40.9**	**18.8**

Table S2. Comparison of the electrochemical performances normalized based on geometric area and volume of MSCs fabricated by various techniques.

References	Preparation Method	System	Thickness (μm)	Areal Capacitance (mF cm^{-2})	Volumetric Capacitance (F cm^{-3})	Areal Power Density (mW cm^{-2})	Areal Energy Density (μWh cm^{-2})	Volumetric Power Density (W cm^{-3})	Volumetric Energy Density (mWh cm^{-3})
28	Supersonic cluster beam printing	Nanostructured carbon	0.2	0.14 (80 μA cm^{-2})	7 (80 μA cm^{-2})	0.2	0.05	10	2.5
29	Laser-scribed	Laser-scribed graphene	7.6	2.32 (16.8 mA cm^{-3})	3.05 (16.8 mA cm^{-3})	152	1.52	200	2
30	Pen drawing and electrodepositing	MnO_2	2	26.6 (0.1 mA cm^{-2})	53.2 (0.1 mA cm^{-2})	~0.2	0.94	~1	4.7
31	Layer-by-layer	MWNTs/Mn_3O_4	0.22	0.63 (10 mV s^{-1})	29 (10 mV s^{-1})	0.506	0.0572	23	2.6
32	Layer-by-layer	MWNT-Mn_3O_4	0.605	0.54 (0.1 A cm^{-3})	8.9 (0.1 A cm^{-3})	0.266	0.109	4.4	1.8
33	Vacuum filtration and thermal reduction	RGO/MnO_2/AgNW	0.06	0.027 (10 mV s^{-1})	4.42 (10 mV s^{-1})	~0.18	0.0138	~30	2.3
34	Vacuum-filtrating and transfer.	Titanium carbide	0.51	0.03024 (0.288 A cm^{-3})	1.44 (0.288 A cm^{-3})	0.0143	0.0102	~0.28	0.2
35	Laser printing and vacuum-assisted deposition	MXene	2.2	27.29 (0.25 mA cm^{-2})	124 (0.25 mA cm^{-2})	0.187	1.342	0.85	6.1
36	CO_2 laser machining and spray-coating	Mxene	4	23 (0.1 mA cm^{-2})	57.5 (0.1 mA cm^{-2})	0.298	1.12	0.744	2.8
37	Meyer rod coated and laser machining	Ti_3C_2 MXene	125	25 (20 mV s^{-1})	2 (20 mV s^{-1})	46.6	0.77	3.728	0.0616
38	Dip coating and scalpel engravin	$Ti_3C_2T_x$ MXene	0.15	0.283 (20 mV s^{-1})	18.9 (20 mV s^{-1})	0.1	0.01	~6.67	~0.67

39	Spray coating	$Ti_3C_2T_x$ and rGO	0.3	2.4 (2 mV s^{-1})	80 (2 mV s^{-1})	0.33	0.258	11	8.6
This work	**Screen printing**	**RuO_2/AgNW/rGO**	**0.71**	**26 (1 mV s^{-1})**	**338 (1 mV s^{-1})**	**2.9**	**1.33**	**40.9**	**18.8**

References

1 N. Liu and Y. Gao, *Small*, 2017, **13**, 1701989.

2 X. Shi, Z.-S. Wu, J. Qin, S. Zheng, S. Wang, F. Zhou, C. Sun and X. Bao, *Adv. Mater.*, 2017, **29**, 1703034.

3 K.-H. Chang, C.-C. Hu and C.-Y. Chou, *Chem. Mater.*, 2007, **19**, 2112-2119.

4 V. K. A. Muniraj, C. K. Kamaja and M. V. Shelke, *ACS Sustain. Chem. Eng.*, 2016, **4**, 2528-2534.

5 S. Kong, K. Cheng, T. Ouyang, Y. Gao, K. Ye, G. Wang and D. Cao, *Electrochim. Acta*, 2017, **246**, 433-442.

6 A. Salomonsson, R. M. Petoral, K. Uvdal, C. Aulin, P.-O. Käll, L. Ojamäe, M. Strand, M. Sanati and A. L. Spetz, *J. Nanopart. Res.*, 2006, **8**, 899-910.

7 B. Hudec, K. Hušeková, A. Rosová, J. Šoltýs, R. Rammula, A. Kasikov, T. Uustare, M. Mičušík, M. Omastová, J. Aarik and K. Fröhlich, *J. Phys. D: Appl. Phys.*, 2013, **46**, 385304.

8 W. Wang, S. Guo, I. Lee, K. Ahmed, J. Zhong, Z. Favors, F. Zaera, M. Ozkan and C. S. Ozkan, *Sci. Rep.*, 2014, **4**, 4452.

9 K. H. Chang and C. C. Hu, *Appl. Phys. Lett.*, 2006, **88**, 193102.

10 M. F. Elkady and R. B. Kaner, *Nat. Commun.*, 2013, **4**, 1475.

11 Y. Yue, Z. Yang, N. Liu, W. Liu, H. Zhang, Y. Ma, C. Yang, J. Su, L. Li and F. Long, *ACS Nano*, 2016, **10**, 11249-11257.

12 G. Lee, D. Kim, D. Kim, S. Oh, J. Yun, J. Kim, S. S. Lee and J. S. Ha, *Energy Environ. Sci.*, 2015, **8**, 1764-1774.

13 Y. Liu, B. Zhang, Q. Xu, Y. Hou, S. Seyedin, S. Qin, G. G. Wallace, S. Beirne, J. M. Razal and J. Chen, *Adv. Funct. Mater.*, 2018, **28**, 1706592.

14 Y. Wang, Y. Shi, C. X. Zhao, J. I. Wong, X. W. Sun and H. Y. Yang, *Nanotechnology*, 2014, **25**, 094010.

15 K. Shen, J. Ding and S. Yang, *Adv. Energy Mater.*, 2018, **8**, 1800408.

16 L. Li, E. B. Secor, K.S. Chen, J. Zhu, X. Liu, T. Z. Gao. J.-W. T. Seo, Y. Zhao and M. C. Hersam, *Adv. Energy Mater.*, 2016, **6**, 1600909.

17 W. J. Hyun, E. B. Secor, C. H. Kim, M. C. Hersam, L. F. Francis and C. D. Frisbie, *Adv. Energy Mater.*, 2017, **7**, 1700285.

18 Y. G. Zhu, Y. Wang, Y. Shi, J. I. Wong and H. Y. Yang, *Nano Energy*, 2014, **3**, 46-54.

19 S. Liu, J. Xie, H. Li, Y. Wang, H. Y. Yang, T. Zhu, S. Zhang, G. Cao and X. Zhao, *J. Mater. Chem. A*, 2014, **2**, 18125-18131.

20 Y. Xiao, L. Huang, Q. Zhang, S. Xu, Q. Chen and W. Shi, *Appl. Phys. Lett.*, 2015, **107**, 013906.

21 Q. Zhang, L. Huang, Q. Chang, W. Shi, L. Shen and Q. Chen, *Nanotechnology*, 2016, **27**, 105401.

22 W. Li, Y. Li, M. Su, B. An, J. Liu, D. Su, L. Li, F. Li and Y. Song, *J. Mater. Chem. A*, 2017, **5**, 16281-16288.

23 G. Sun, J. An, C. K. Chua, H. Pang, J. Zhang and P. Chen, *Electrochem. Commun.*, 2015, **51**, 33-36.

24 J. Li, S. Sollami Delekta, P. Zhang, S. Yang, M. R. Lohe, X. Zhuang, X. Feng and M. Östling, *ACS Nano*, 2017, **11**, 8249-8256.

25 W. Liu, C. Lu, H. Li, R. Y. Tay, L. Sun, X. Wang, W. L. Chow, X. Wang, B. K. Tay, Z. Chen, J. Yan, K. Feng, G. Lui, R. Tjandra, L. Rasenthiram, G. Chiu and A. Yu, *J. Mater. Chem. A*, 2016, **4**, 3754-3764.

26 H. Pang, Y. Zhang, W.-Y. Lai, Z. Hu and W. Huang, *Nano Energy*, 2015, **15**, 303-312.

27 H. Jung, C. Ve Cheah, N. Jeong and J. Lee, *Appl. Phys. Lett.*, 2014, **105**, 053902.

28 L. G. Bettini, A. Bellacicca, P. Piseri and P. Milani, *Flex. Print. Electron.*, 2017, **2**, 025002.

29 M. F. El-Kady and R. B. Kaner, *Nat. Commun.*, 2013, **4**, 1475-1483.

30 K. Guo, Y. Wan, N. Yu, L. Hu, T. Zhai and H. Li, *Energy Storage Materials*, 2018, **11**, 144-151.

31 S. Y. Hong, J. Yoon, S. W. Jin, Y. Lim, S.-J. Lee, G. Zi and J. S. Ha, *ACS Nano*, 2014, **8**, 8844-8855.

32 G. Lee, D. Kim, D. Kim, S. Oh, J. Yun, J. Kim, S.-S. Leea and J. S. Ha, *Energy Environ. Sci.*, 2015, **8**, 1764-1774.

33 W. Liu, C. Lu, X. Wang, R. Y. Tay and B. K. Tay, *ACS Nano*, 2015, **9**, 1528-1542.

34 B.-S. Shen, H. Wang, L.-J. Wu, R.-S. Guo, Q. Huang and X.-B. Yan, *Chin. Chem. Lett.*, 2016, **27**, 1586-1591.

35 H. Hu and T. Hua, *J. Mater. Chem. A*, 2017, **5**, 19639-19648.

36 Q, Jiang, C. Wu, Z. Wang, A. C. Wang, J.-H. He, Z. L. Wang and H. N. Alshareef, *Nano Energy*, 2018, **45**, 266-272.

37 N. Kurra, B. Ahmed, Y. Gogotsi and H. N. Alshareef, *Adv. Energy Mater.*, 2016, **6**, 1601372.

38 P. Salles, E. Quain, N. Kurra, A. Sarycheva and Y. Gogotsi, *Small*, 2018, **14**, 1802864.

39 C. Couly, M. Alhabeb, K. L. Van Aken, N. Kurra, L. Gomes, A. M. Navarro-Suárez, B. Anasori, H. N. Alshareef and Y. Gogotsi, *Adv. Electron. Mater.*, 2017, **4**, 1700339.